PFC/JA-84-16

IMPURITY DENSITY CALCULATIONS FROM SPECTROSCOPIC MEASUREMENTS OF VISIBLE AND UV LINE EMISSION ON THE ALCATOR C TOKAMAK

Juan C. Moreno, Earl S. Marmar

Plasma Fusion Center
Massachusetts Institute of Technology
Cambridge, MA 02139

June 6, 1984

This work was supported by the U.S. Department of Energy Contract No. DE-AC02-78ET51013. Reproduction, translation, publication, use and disposal, in whole or in part by or for the United States government is permitted.

Impurity Density Calculations from Spectroscopic Measurements of Visible and UV Line Emission on the Alcator C Tokamak

J. C. Moreno and E. S. Marmar

Plasma Fusion Center, M.I.T. Cambridge, MA 02139

ABSTRACT

Densities of C, O, and Si during the steady state portion of Alcator C discharges have been computed from spectroscopic measurements of the absolute brightnesses of visible and UV emission lines in combination with with a 1-D transport calculation which models the charge state and emissivity profiles. Profiles of all the charge states of a particular impurity were calculated by utilizing independent measurements of plasma density and temperature and solving the coupled system of transport and rate equations connecting the ionization states. These profiles were then used to calculate emissivity profiles by solving the matrix equation relating the level populations through collisional excitation, collisional de-excitation, spontaneous emission, innershell ionization and cascades from upper levels. Three different types of limiters, molybdenum, graphite and SiC coated graphite, have been used on Alcator C. It was observed that the principal impurities in the plasma, under most conditions, were determined by the type of limiter material being used. However, the source of the impurities could be either the wall or the limiters, since it has been shown that the wall becomes coated with limiter material. A significant influx of impurities directly from the limiters was often seen during the application of lower hybrid RF power to the plasma.

I. INTRODUCTION

The density and spatial distribution of impurities in a tokamak discharge can greatly influence the characteristics of the plasma. Even a modest amount of impurities can affect energy confinement, especially the heavier impurities which do not become fully stripped and radiate mostly from the central region of the plasma. Too large a concentration of impurities can cause disruptions or result in considerable radiative power loss [1]. For these reasons it is essential that plasmas in reactor relevant regimes be kept clean ($Z_{eff} \sim 1$). However, small amounts of light impurities can be tolerated, and may in fact be beneficial, since they radiate from the edge region of the plasma and should therefore help keep the temperature at the edge low. This, in turn, can reduce sputtering from edge structures [2]. Spectroscopic instruments, operating from the visible to the x-ray region of the spectrum, are typically used to study impurities in tokamak plasmas [3-5]. The principal instrument used in this experiment is a spectrograph covering the visible and UV portion of the spectrum (2000 Å - 8000 Å). Additionally, some of the data presented are from measurements taken using vacuum UV monochromators.

In Section II, the spectrograph and the Alcator C tokamak will be described in more detail. A brief survey will also be given of diagnostics that routinely operate on Alcator. Section III contains an explanation of the theoretical model and numerical computations which were used to obtain absolute impurity densities. Section IV shows typical examples of emissivity, brightness and impurity density profiles, calculated from the numerical simulations. Finally, Section V contains a study of how

impurity emission from Alcator C depends on the type of limiter material being used. A comparision is shown of low - medium Z impurities resulting from molybdenum, graphite and SiC coated graphite limiters. The influx of impurities into the plasma during lower hybrid RF heating is also examined.

II. EXPERIMENTAL ARRANGEMENT

Most of the measurements reported here have been obtained using a 1.5 meter grating spectrograph with a Wadsworth mounting. The instrument has a reciprocal linear dispersion of nominally 10.8 Å/mm in first order using a concave holographic grating with 600 G/mm. One of the advantages of this instrument's wavelength range is that no vacuum is needed and the absolute calibration, using a tungsten lamp, is straightforward and relatively accurate. The disadvantage is that it is more difficult, theoretically, to obtain impurity densities from the characteristic lines in this part of the spectrum, because the emission is mostly from the edge region of the plasma where there is more turbulence and the plasma parameters are less well known. In addition, as will be discussed later, poloidal and toroidal asymmetries are generally important. There are two modes of operation for this spectrograph. The first consists of using a film attachment that can take film spectra in the range 2000 Å - 8000 Å. Film spectra were recorded every few months in order to obtain a survey of the emission lines and verify which impurities were present in the plasma. A portion of a densitometer trace of one such spectrum is shown in fig. 1. In the usual mode of operation, the absolute brightnesses of emission lines were measured as a function of time. Up to 10 emission lines were recorded simultaneously by sending the light through

quartz optical fibers to PM tubes as shown in fig. 2. The fiber arrays are connected at one end to a brass plate which attaches along the exit plane of the spectrograph. Slots had been milled into the plate at the locations where chosen emission lines were focused on the exit plane. The fibers transfer the light passing through the slots to the photomultiplier tubes, whose output signals are then digitized and stored on a computer.

Measurements from other diagnostics were used to supplement the spectrograph data. Two vacuum UV monochromators were utilized: one is a grazing incidence monochromator covering the wavelength range 50 Å -500 Å; the other is a normal incidence monochromator covering the range 1200 Å - 2300 Å. Electron density is measured on Alcator C using a five chord laser interferometer [6]. Electron temperatures are measured by Thomson scattering, ECE emission [7] and soft x-ray emission [8].

The Alcator C tokamak is a high field, high density plasma confinement device which has a major radius of 64 cm and a minor radius of 16.5 cm. A typical discharge for which these data were taken had the following conditions: toroidal field B_T = 80 kG; line average electron density $\bar{N}_e = 2 \times 10^{14}$ cm^{-3}; central electron temperature T_e = 1500 eV; plasma current Ip = 450 kA. The range of plasma parameters is B_T = 40 - 120 kG, $\bar{N}_e = 1 \times 10^{13} - 1 \times 10^{15}$ cm^{-3} and T_e = 1 - 3 keV.

Characteristic time histories of impurity lines are shown in fig. 3. They consist of an ionization spike at the beginning of the discharge when the plasma is rapidly being heated and then, after about 10 msec, the ionization states reach a steady state equilibrium [9]. It was during this steady state portion of the discharge that the impurity densities were calculated.

Impurity concentrations were computed for only a limited range of plasma densities, $1 \times 10^{14}\ cm^{-3} < \bar{N}_e < 2 \times 10^{14}\ cm^{-3}$, where the plasma was well behaved and its parameters could be accurately measured. An example of the variation of C III and C V brightnesses with line average electron density can be seen in fig. 4. For $\bar{N}_e < 1 \times 10^{14}\ cm^{-3}$, the plasma exhibits non-thermal effects and the dominant contribution to Z_{eff} is from heavier impurities (with molybdenum limiters), while for $\bar{N}_e > 2 \times 10^{14}\ cm^{-3}$ the plasma experiences what are referred to as 'marfes'. A 'marfe' is believed to be a thermal instability which results in a poloidally asymmetric high density region of plasma near the limiter radius and usually close to the inside major radius edge of the plasma [10].

III. NUMERICAL MODELING: THEORY

The method used here to obtain impurity densities begins with the determination of the theoretical charge state profiles based upon the measured electron density and temperature profiles and an impurity transport model. A good review of different transport models can be found in [11]. Charge state profiles as a function of time are computed first by solving the coupled system of transport and rate equations [12,13] connecting the ionization states:

$$\frac{\partial N^1(r,t)}{\partial t} = -N_e N^1 I(1,2) + N_e N^2 R(2,1) - \nabla \cdot \Gamma^1 + N_o\, \delta(t) \qquad (1)$$

$$\frac{\partial N^2(r,t)}{\partial t} = N_e N^1 I(1,2) - N_e N^2 I(2,3) + N_e N^3 R(3,2) - N_e N^2 R(2,1) - \nabla \cdot \Gamma^2$$

$$\vdots \qquad\qquad \vdots$$

$$\frac{\partial N^z(r,t)}{\partial t} = N_e N^{z-1} I(z-1,z) - N_e N^z R(z,z-1) - \nabla \cdot \Gamma^z$$

$$\Gamma^i(r) = -D\,\nabla N^i - N^i v$$

$$v(r) = v_a r/r_L$$

$$D(r) = \text{Const.}$$

where N^i is the density of the ith ionization state, N_o is the initial density of the singly ionized impurity, Γ^i is the flux, I(i,j) is the ionization rate [14] from charge state i to state j, R(i,j) is the recombination rate [15], D is the diffusion coefficient, v(r) is the convection velocity, v_a is a constant, r_L is the minor radius and z is the nuclear charge. Impurity injection experiments performed on Alcator A and C [16] showed that impurity transport was inconsistent with neoclassical theory and instead could be described solely by an anomalous diffusion term or by diffusion plus a small amount of convection. Empirical relationships for the confinement time τ and the diffusion coefficient D, as a function of various plasma parameters, were determined. These formulas for τ and D, which assumed no inward convection, were initially used in the computation. To investigate the effects of convection, an analytical expression for the confinement time is employed [17],

$$\tau = \frac{77 + S^2}{56 + S^2} \quad \frac{e^S - S - 1}{4S^2} \quad \frac{r_L^2}{D} \quad \text{sec} \qquad (2)$$

where S is the dimensionless "convection parameter" given by $S = r_L\, v_a/2D$. Effects of convection can be included by choosing an appropriate value for

v_a and adjusting D so that the confinement time given by equation (2) remains the same.

Finding a steady state solution of equation (1) requires choosing an initial distribution for the singly ionized impurity (typically a gaussian of width .5 cm with a peak near the limiter radius). The equations are then integrated for several confinement times until essentially all the particles are lost. The time integral density profiles are solutions for a steady state source. The integral equations representing the steady state solution are

$$N^i(r,t) = \int_o^t N^{i*}(r,t')dt' \qquad (3)$$

where $N^{i*}(r,t')$ is the solution to equation (1) and i = 1 to z.

Once the charge state profiles have been computed, the next step in the calculation of the absolute charge state density is to compute the emissivity and brightness profiles and then finally to normalize all the profiles to the measured central chord brightness of an emission line. The intensity of the emission lines observed here are determined mainly by electron impact excitation and spontaneous decay between the separate energy levels of the ion. Rate coefficients [18-23] for each of the individual transitions, from quantum number n = 1 to n = 3 or 4, are used in the calculations. Higher n levels have been included by using expressions for average spontaneous decay rates and average excitation rates. The emissivity of a photon is directly related to the density of the excited state from which the line was emitted, through the relation $E(p,q) = N^z(p)A(p,q)$ where A(p,q) is the spontaneous decay rate [24,25]

from level p to q and $N^z(p)$ is the density of level p in charge state z. Using the density of this excited state and assuming steady state, a matrix representing a system of m equations is solved to determine the density of all the individual energy levels up to n = 4 and the average density for n > 4. The equations are

$$\frac{\partial N^z(2;r)}{\partial t} = 0 = \sum_p N^z(p)A(p,2) - N^z(2)A(2,1) + N_e \sum_p N^z(p)X(p,2)$$
$$- N_e N^z(2) \sum_p X(2,p) + N_e N^{z-1} I_c(z-1,z;2) \qquad (4)$$

$$\frac{\partial N^z(3;r)}{\partial t} = 0 = \sum_p N^z(p)A(p,3) - N^z(3) \sum_p A(3,p) + N_e \sum_p N^z(p)X(p,3)$$
$$- N_e N^z(3) \sum_p X(3,p) + N_e N^{z-1} I_c\ (z-1,z;3)$$

$$\vdots \qquad\qquad \vdots$$

$$\frac{\partial N^z(m+1;r)}{\partial t} = 0 = -N^z(m+1) \sum_p A(m+1,p) + N_e \sum_p N^z(p)X(p,m+1)$$

where X(p,q) is the collisional excitation (or de-excitation) rate from level p to q and I_c is the collisional innershell ionization rate. Note that it is not necessary to include the equation for the ground state density since the density of one of the excited states is computed directly from the measured brightness of an emission line.

Level populations (for n < 4) are determined principally by spontaneous decay and electron impact excitation among low n energy levels. However, collisional innershell ionization and cascading from high n levels also influence, to a lesser degree, the level populations and have therefore been included in the calculations. Dielectronic recombination and charge exchange have been neglected here. These processes could be

important in determining the population of high n energy levels but will have negligible effect on the intensities of the measured lines.

Collisional innershell ionization is an atomic process where ionization occurs through the loss of an innershell electron, leaving the ion in an excited state. Only ionization to the first few excited states of an ion has been considered. An important case is innershell ionization from the ground state of a Li-like ion to the first excited state of a He-like ion.

Excited states with high quantum numbers ($n > 4$) can influence the population of low n states through cascades. This effect has been taken into account by using average transition rates between quantum levels n_i and n_j. The average spontaneous decay rate [26] is given by

$$\bar{A}(n_j,n_i) = \frac{1.57 \times 10^{10}\ Z_c^{\,4}}{n_i n_j^{\,3}(n_j^{\,2} - n_i^{\,2})} \quad \text{sec}^{-1} \tag{5}$$

where Z_c is the effective nuclear charge. The average collisional excitation rate is taken to be [27]

$$\bar{X}(n_i,n_j) = \frac{1.58 \times 10^{-5}\ \bar{f}\ \langle g\rangle \exp(-\Delta E/T_e)}{\Delta E\ T_e^{\,1/2}} \quad \text{cm}^3/\text{s} \tag{6}$$

where $\langle g\rangle$ is the average gaunt factor, ΔE is the difference in energy between level i and level j, and $\bar{f}$ is an average oscillator strength given by

$$\bar{f}(n_i,n_j) = \frac{1.96}{n_i^{\,2} n_j^{\,3}} \left(\frac{1}{n_i^{\,2}} - \frac{1}{n_j^{\,2}}\right)^{-3} \tag{7}$$

Including these higher n excited levels changes the computed density of ionization states, particularly those with metastable levels (e.g. C III, O V). This is due to the fact that these ions with metastable states have

a relatively large population in the high n energy levels and therefore cascades can appreciably populate the low energy levels.

Equation (4) was represented by a matrix and solved every 0.1 cm along the minor radius with the input initially being a radially constant emissivity profile of the measured emission line. The solution at each radial location yielded the densities of the energy levels, which were then added together to give the total charge state density. This charge state density was made to agree with the charge state profile obtained from equation (3) by adjusting the emissivity profile. By repeating this procedure iteratively it was possible to obtain an emissivity profile which was self-consistent with the charge state profile and also normalized to the measured central chord brightness.

IV. NUMERICAL MODELING: RESULTS

The numerical model and the absolute brightnesses of emission lines were used to determine densities of impurities for a wide range of plasma conditions and with three types of limiters: molybdenum; graphite; and SiC coated graphite. For plasma densities above $\bar{N}_e = 1 \times 10^{14}$ cm^{-3}, the dominant impurities in ohmically heated Alcator C discharges were found to be carbon, oxygen, and silicon, depending on the limiter being used. The main emission lines used to calculate densities were C III (4650 Å), C IV (1550 Å), C V (2271 Å), O V (2781 Å), Si III (4552 Å) and Si XI (303 Å). Measured brightnesses of the lines were reproducible from shot to shot if the plasma density and current were kept constant and no major disruptions occurred. Variations in plasma conditions, and the application of lower hybrid RF power [28], were found to influence significantly the impurity level in the plasma. The impurity calculation de-

scribed in the previous section requires independent measurements of electron temperature and density profiles (fig. 5). The electron temperature profile has been studied extensively on Alcator C by measuring second harmonic electron cyclotron emission [7] and under most conditions the profile is well approximated by a gaussian of width a_T given by

$$a_T = \left(\frac{3}{2}\ \frac{q_o}{q_L}\right)^{1/2} r_L \quad \text{cm} \tag{8}$$

where q_o is the safety factor on axis and q_L is the safety factor at the limiter radius. The electron density profile as measured by a laser interferometer is roughly described by a parabolic function, $(1-(r/a)^2)^m$, where m is typically between .5 and 1. The temperature and density in the shadow of the limiter, where the lowest charge states exist, have been measured with Langmuir probes [29] and it was found that T_e is nearly constant in this region while N_e decreased exponentially in radius with a scrape-off length of typically .3 cm.

A representative plasma shot (using graphite limiters) is shown in fig. 6, where the top trace is the plasma current, the second trace is the central chord averaged electron density, the third trace is the central soft x-ray emission (photon energy > 1 keV) and the bottom trace is the continuum emission near 5360 Å, due primarily to free-free bremsstrahlung. For these steady state plasma conditions, fig. 7 shows the simulated charge state profiles for carbon calculated with the transport code (assuming v_a = 0 cm/s, D = 3400 cm^2/s). Including modest inward convection causes the profile of fully ionized low Z impurities to be more peaked, while partially ionized species are only slightly affected. Fig. 8 shows a plot of the total C density for S = 0, S = 1/2 and S = 1.

The amount of convection usually chosen is S ~ 1/2, which yields a flat Z_{eff} profile, consistent with profiles from visible bremsstrahlung measurements [30].

The brightnesses of lines from more than one charge state of each impurity were used to calculate the impurity density. Agreement between the calculated densities from using different emission lines was in general within a factor of two. It should be noted however that the agreement was good only for the plasma density range 1×10^{14} cm^{-3} < $\bar{N}_e$ < 2×10^{14} cm^{-3}. The numerical model becomes unreliable outside of this range, particularly for the low charge states, for the reasons described earlier. Poloidal and toroidal asymmetries in line emission [31-33] could also be a source of error for the low charge states. Computed emissivity and brightness profiles for C III and C V are shown in fig. 9. The accuracy of these profiles are of course dependent on the reliability of the ionization, recombination, excitation and spontaneous decay rates. By running the code with different values for the atomic rates it was estimated that the error arising from the uncertainties in atomic rates is less than a factor of two. Assuming C was the only impurity (using graphite limiters), Z_{eff} calculated from the total C density was about 1.3, which agreed within experimental uncertainty with the value obtained from visible bremsstrahlung measurements, which was Z_{eff} = 1.5.

V. LIMITER STUDIES

Experiments were conducted on Alcator C to investigate changes in impurity concentrations during the use of different types of limiters. Table I shows computed densities and Z_{eff} values of C, O and Si under similar plasma conditions for four periods of time when three different

limiter sets were used. The limiters that were initially used on Alcator C for several years were made of molybdenum. Spectroscopic measurements made during the use of molybdenum limiters revealed that the O and C density for a typical run were comparable, and lesser amounts of N were also present. When graphite limiters were installed in the device, the C density increased a factor of four, while the O density immediately decreased a factor of ten, leaving Z_{eff} unchanged. A similar lack of oxygen was observed in the TM-G experiment, where the entire first wall was constructed from graphite [35]. Switching back to molybdenum limiters after several months of operation with graphite limiters resulted in only a slight decrease in C density indicating that the walls were now a significant source of C entering the plasma. A gradual increase of O density occurred over the period of several weeks with the Mo limiters. Next, a SiC coated graphite limiter was installed on Alcator C. It was found that the dominant impurity was C, whose density was typically a factor of ten or more larger than Si. Although no quantitative study has been made here of Mo density in Alcator C, it has been observed previously [34] that Mo also becomes deposited on the wall and will remain in the machine even after the Mo limiters are removed. However, Mo only plays a significant role in discharges with $\overline{N}_e < 1 \times 10^{14}$ and while using Mo limiters.

The application of lower hybrid RF auxiliary heating to the discharge resulted in increased impurity levels, particularly for RF power > 500 kW, where Z_{eff} increased strongly with power [28]. Fig. 10 shows a plasma shot with LHRF heating (RF power = 800 kW), in which T_e increased by 500 eV. It was observed that, in the course of an RF pulse, the emission from higher ionization states of Si and C increased substantially (depending on plasma density and RF power), while a smaller relative effect was

seen for the lower ionization states. This increase in impurity emission can not be accounted for by the increase in T_e. However, it is consistent with assuming that the source of Si and C from the wall is at least comparable to the source from the limiters during a normal ohmic discharge, but the limiters become the main source of impurities when LHRF is turned on. The lower charge states show less of a relative increase in brightness during RF than the higher charge states because an impurity coming off the limiter will be partially ionized before it can travel toroidally to where it can be viewed by one of the spectrometers, which were at non-limiter ports. Limiters were placed 180° apart toroidally while the ports are located every 60° toroidally. The densities of Si and C during the RF pulse were estimated by the increase in brightness of Si XI and C V lines. This method gave a lower limit to the increase in impurity density because of the substantial toroidal asymmetry of edge impurity emission during RF. An unusually large injection of Si and C, after RF is applied, can be seen in fig. 11, where even the low charge states show a marked increase in brightness.

VI. CONCLUSIONS

The principal impurities measured in Alcator C plasmas for $\bar{N}_e > 1 \times 10^{14}$ cm^{-3} were C, O and Si. Impurity densities were calculated with a numerical simulation consisting of two parts, first a transport model that computes charge state profiles and second a model determining the level populations of each charge state. These two models were combined, along with absolute brightness measurements of impurity lines, to determine impurity density profiles of all charge states. Impurity densities showed consistency among brightnesses of lines from different charge states of the same

element, and also showed reasonable agreement with independent measurements of Z_{eff}. The walls were a significant, if not the main source of low Z impurities during a typical ohmic discharge. An interesting effect was the large decrease in oxygen concentration when Mo limiters were replaced by graphite. Depositing LHRF power into the plasma resulted in a significant influx of impurities from the limiters. The increase of Z_{eff} with lower hybrid heating was particularly strong for LHRF power > 500 kW.

ACKNOWLEDGEMENTS

We wish to thank J. Terry for useful comments and discussions. The assistance of the rest of the Alcator group is also gratefully acknowledged. This work was supported by U. S. Department of Energy Contract Number DE-AC02-78ET51013.

REFERENCES

[1] R.V. Jensen, D.E. Post, W.H. Grasberger, C.B. Tarter and W.A. Locke, Nuclear Fusion, 14, 289 (1974).

[2] G.M. McCracken and P.E. Stott, Nuclear Fusion, 19, 889 (1979).

[3] Equipe TFR, Nuclear Fusion, 18, 647 (1978).

[4] C. Breton, C. DeMichelis and M. Mattioli, "Spectroscopic Study of Ohmically Heated Tokamak Discharges", Fontenay-Aux-Roses, Report EUR-CEA-FC-1060, July 1980.

[5] C. DeMichelis and M. Mattioli, Nuclear Fusion, 21, 677 (1981).

[6] S.M. Wolfe, K.J. Button, J. Waldman and D.R. Cohn, Appl. Optics, 15, 2645 (1976).

[7] S.E. Kissel, "Thermal & Non-Thermal Submillimetre Emission from Alcator Tokamak", Ph.D. Thesis, PFC Report PFC/RR-82-15, June 1982.

[8] J.E. Rice, private communication (1983).

[9] J.L. Terry, K.I. Chen, H.W. Moos and E.S. Marmar, Nuclear Fusion, 18, 485 (1978).

[10] B. Lipschultz, B. Labombard, E. Marmar, M. Pickrell, J. Terry, R. Watterson and S. Wolfe, "Marfes: An Edge Plasma Phenomenon", Nuclear Fusion, to be published, M.I.T. PFC Report, PFC/JA-83-33, October, 1983.

[11] R.J. Hawryluk, S. Suckewer and P. Hirshman, Nuclear Fusion, 19, 607 (1979).

[12] S.A. Cohen, J.L. Cecchi and E.S. Marmar, Phys. Rev. Lett., 35, 1507 (1975).

[13] E.S. Marmar, Ph.D. Thesis (Princeton), unpublished.

[14] W. Lotz, Astrophys. J. Suppl. 14, 207 (1967).

[15] M. Mattioli, Eurotom-C.E.A. Assoc., Fontenay-Aux-Roses, Report EUR-CEA-FC-761 (1975).

[16] E.S. Marmar, J.E. Rice, J.L. Terry and F.H. Seguin, Nuclear Fusion, 22, 1567 (1982).

[17] F. Seguin, R. Petrasso and E. Marmar, Phys. Rev. Lett., 51, 455 (1983).

[18] N.H. Magee, J.B. Mann, A.L. Merts and W.D. Robb, "Impact Excitation of Carbon and Oxygen Ions",Los Alamos Report, LA-6691-MS (1977).

[19] P.L. Dufton, K.A. Berrington, P.G. Burke and A.E. Kingston, Astron. & Astrophys. 62, 111 (1978).

[20] M. Malinovsky, Astron. & Astrophys., 43, 101 (1975).

[21] K.L. Baluja, P.G. Burke and A.E. Kingston, J. Phys. B. 14, 1333 (1981).

[22] H. Nussbaumer and P.J. Storey, Astron. & Astrophs., 64, 139 (1978).

[23] I.I. Sobelman, L.A. Vainshtein and E.A. Yukov, "Excitation of Atoms and Broadening of Spectral Lines", Springer-Verlag (1981).

[24] W.L. Wiese, M.W. Smith and B.M. Glennon, "Atomic Transition Probabilities", NBS Monograph, NSRDS-NBS 4 (1966).

[25] J. Reader, C.H. Corliss, W.L. Wiese and G.A. Martin, "Wavelengths and Transition Probabilities for Atoms and Atomic Ions", NBS Monograph NSRDS-NBS 68 (1980).

[26] R.D. Cowan, "The Theory of Atomic Structure and Spectra", Univ. of Calif. Press (1981).

[27] M.J. Seaton, Planetary and Space Sci., 12, 55 (1964).

[28] E.S. Marmar, M. Foord, B. Labombard, B. Lipschultz, J. Moreno, et al, "Impurity Generation during Intense Lower Hybrid Heating Experiments on the Alcator C Tokamak", Jour. of Nucl. Mater. to be published, M.I.T. PFC Report PFC/JA-83-37, September 1983.

[29] A. Hayzen, D. Overskei and J. Moreno, "Probe Measurements of the Boundary Plasma in Alcator ", M.I.T. PFC Report, PFC/JA-81-10, April 1981.

[30] M.E. Foord, E.S. Marmar and J.L. Terry, Rev. Sci. Instrum. 53, 1407 (1982).

[31] S.L. Allen, H.W. Moos, R.K. Richards, J.L. Terry and E.S. Marmar, Nuclear Fusion, 21, 251 (1981).

[32] J.L. Terry, E.S. Marmar, K.I. Chen and H.W. Moos, Phys. Rev. Lett., 39, 1615 (1977).

[33] K. Brau, M. Bitter, R.J. Goldston, D. Manos, K. McGuire, S. Suckewer, Nuclear Fusion, 23, 1643 (1983).

[34] J.E. Rice, E.S. Marmar, B. Lipschultz and J.L. Terry, Nuclear Fusion, 24, 329 (1984).

[35] E.I. Dobrokhatov, et al., in Plasma Physics and Controlled Nuclear Fusion Research (Proc. 9th Int. Conf. Balt., 1982) Vol. III, IAEA, 229 (1983).

FIGURE CAPTIONS

Figure 1: Densitometer trace of a film spectra, integrated over several plasma shots

Figure 2: Experimental setup of the visible - UV spectrograph (2000 Å - 8000 Å).

Figure 3: Time evolution of C III, C IV, C V, Si III and Si XI line emissions for an ohmic discharge. I_p = 450 kA, N_e = 2.5×10^{14} cm^{-3} and B_T = 80 kG.

Figure 4: C III and C V plotted as a function of line average electron density with all other plasma parameters remaining constant. I_p = 400 kA and B_T = 100 kG. For line average electron densities above 2×10^{14} cm^{-3} the effect of 'marfes' can be seen in the C III emission.

Figure 5: Typical T_e and N_e profiles used in the impurity calculation.

Figure 6: Typical ohmic discharge. The top trace is the plasma current, the second trace is the line average electron density ($.55 \times 10^{14}$ cm^{-3} / fringe), the third trace is the soft x-ray emission and the bottom trace is the visible continuum emission (5360 Å).

Figure 7: Computed profiles of all the ionized states of C assuming no inward convection (S = 0).

Figure 8: Total C density evaluated for three different values of the convection parameter S.

Figure 9: Computed emissivity and brightness profiles of C III (4650 Å) and C V (2271 Å). The solid lines are brightnesses while the dashed lines are emissivities.

Figure 10: The RF pulse is applied at about 230 msec and stays on for 70 msec. An increase can be seen in C V and Si XI emission while no obvious increase is observed in the lower ionization states.

Figure 11: A significant influx of impurities occurs during the RF pulse. Even the low charge states show an increase in emission during RF, though not as large a relative increase as the higher charge states.

TABLE I. COMPARISION OF IMPURITY DENSITIES FOR DIFFERENT LIMITERS

$\bar{N}_e = 2 \times 10^{14}$ cm^{-3}
$T_e = 1500$ eV
$I_p = 450$ kA
$B_T = 80$ kG

Limiter	C Density (cm^{-3})	O Density (cm^{-3})	Si Density (cm^{-3})	Zeff (calc)
Molybdenum (8/82 - 9/82)	4.5×10^{11}	7.1×10^{11}	*	1.23
Graphite (9/82 - 11/82)	1.7×10^{12}	8.7×10^{10}	*	1.24
Molybdenum (2/83 - 3/83)	1.5×10^{12}	5.9×10^{11}	*	1.34
SiC coated Graphite (5/83 - 6/83)	1.5×10^{12}	7.9×10^{10}	1.8×10^{10}	1.23

* Not observed

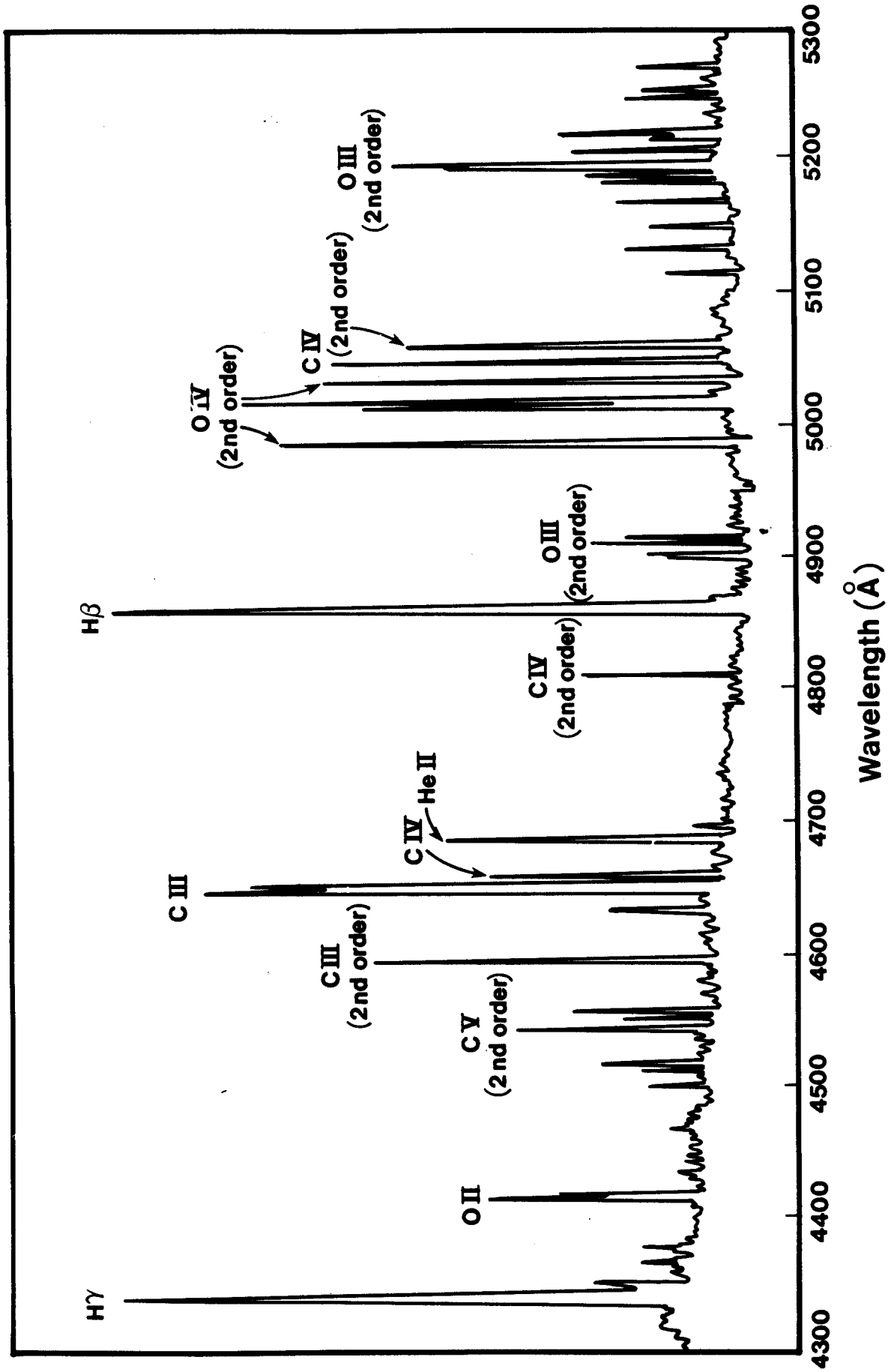
Hγ
OII
CV
(2nd order)
CIII
(2nd order)
CIII
He II
CIV
CIV
(2nd order)
Hβ
OIII
(2nd order)
OIV
(2nd order)
CIV
(2nd order)
OIII
(2nd order)
4300
4400
4500
4600
4700
4800
4900
5000
5100
5200
5300
Wavelength (Å)

FIGURE 1

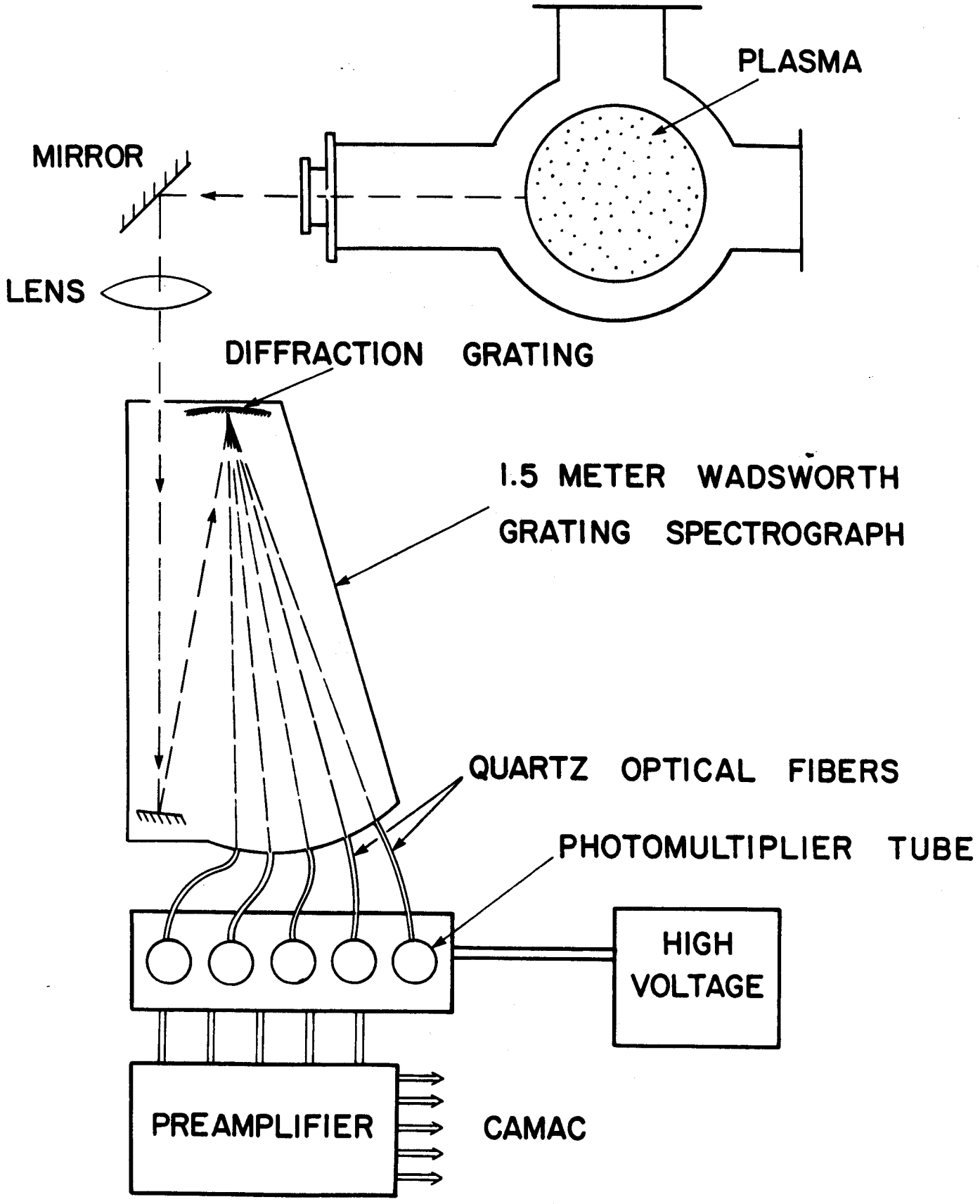
PLASMA
MIRROR
LENS
DIFFRACTION GRATING
1.5 METER WADSWORTH
GRATING SPECTROGRAPH
QUARTZ OPTICAL FIBERS
PHOTOMULTIPLIER TUBE
HIGH
VOLTAGE
PREAMPLIFIER
CAMAC
PFC-8027

FIGURE 2

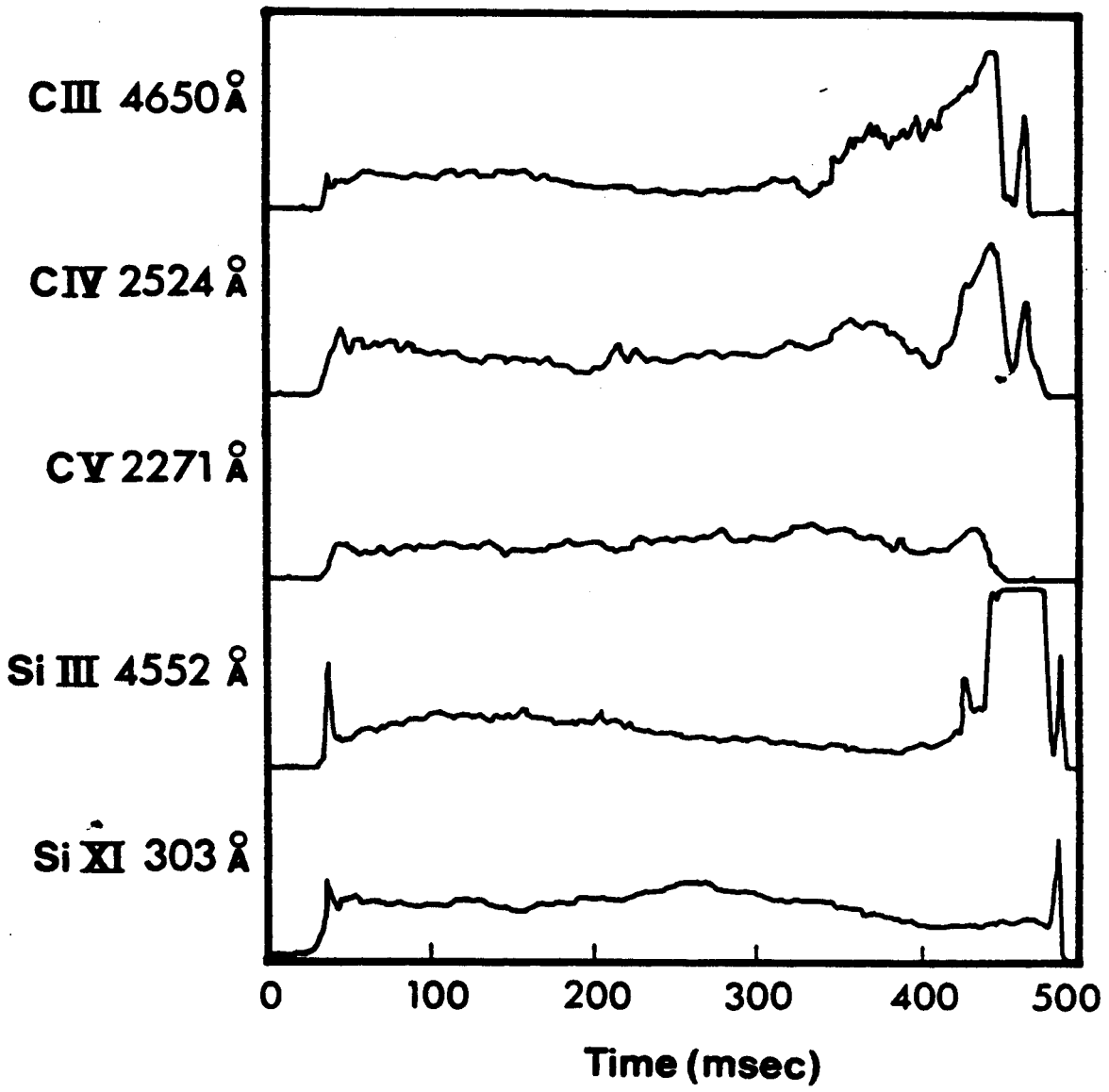
C III 4650 Å
C IV 2524 Å
C V 2271 Å
Si III 4552 Å
Si XI 303 Å
0
100
200
300
400
500
Time (msec)

FIGURE 3

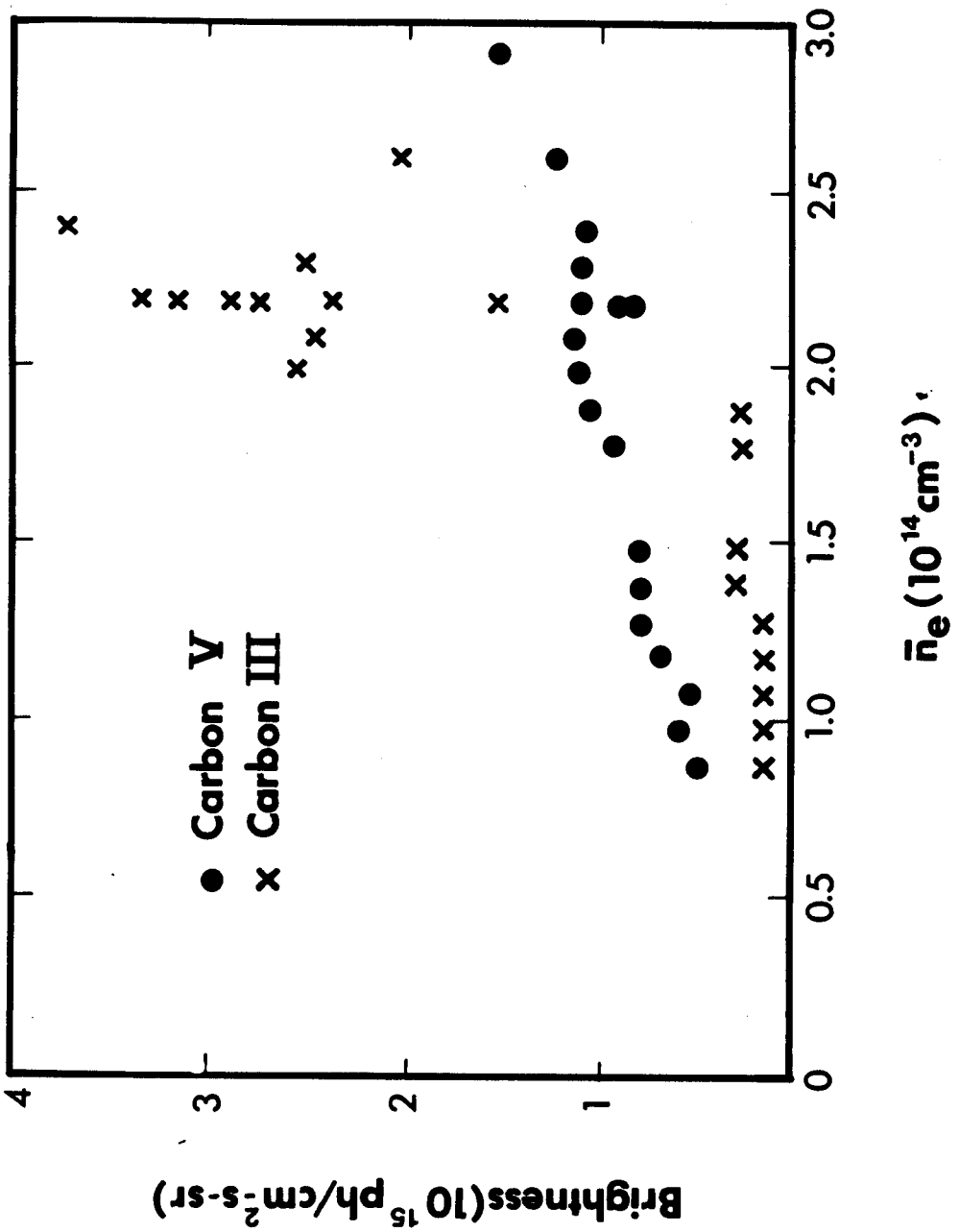
Carbon V
Carbon III
Brightness(10^{15} ph/cm^2-s-sr)
$\bar{n}_e$ (10^{14}cm^{-3})
0
0.5
1.0
1.5
2.0
2.5
3.0
1
2
3
4

FIGURE 4

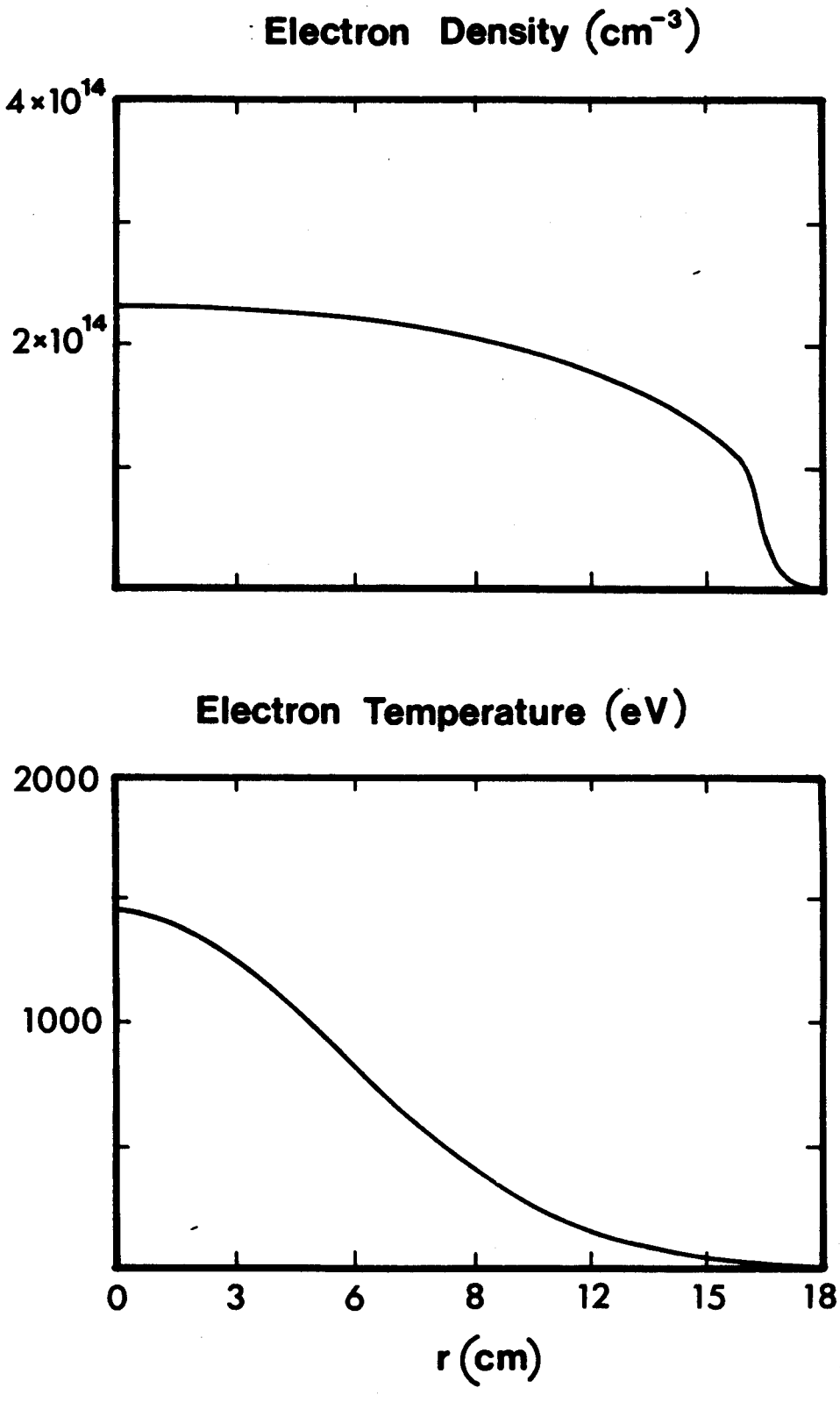
Electron Density (cm^{-3})
4×10^{14}
2×10^{14}
Electron Temperature (eV)
2000
1000
0
3
6
8
12
15
18
r (cm)

FIGURE 5

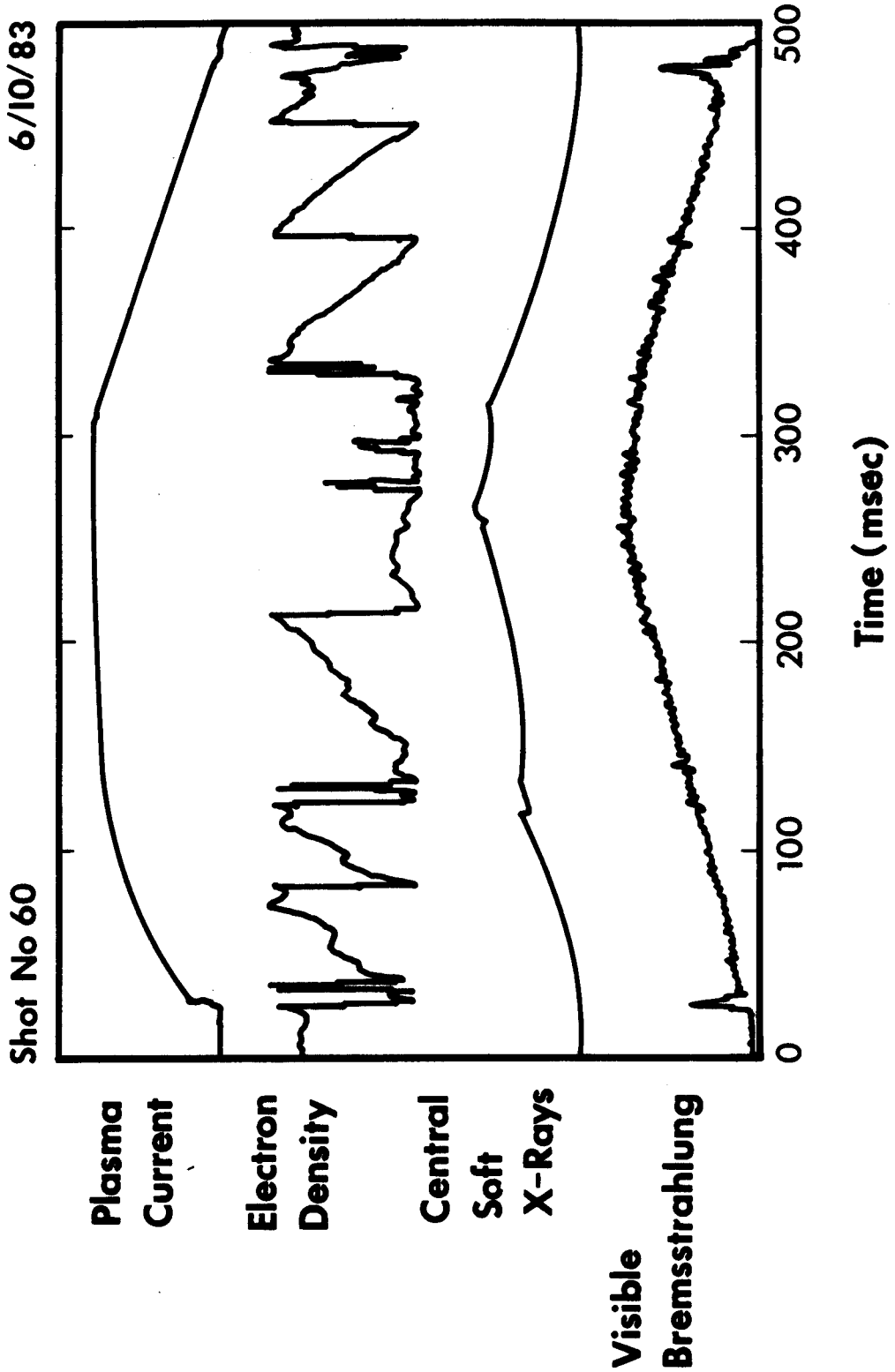
Shot No 60
6/10/83
Plasma Current
Electron Density
Central Soft X-Rays
Visible Bremsstrahlung
0
100
200
300
400
500
Time (msec)

FIGURE 6

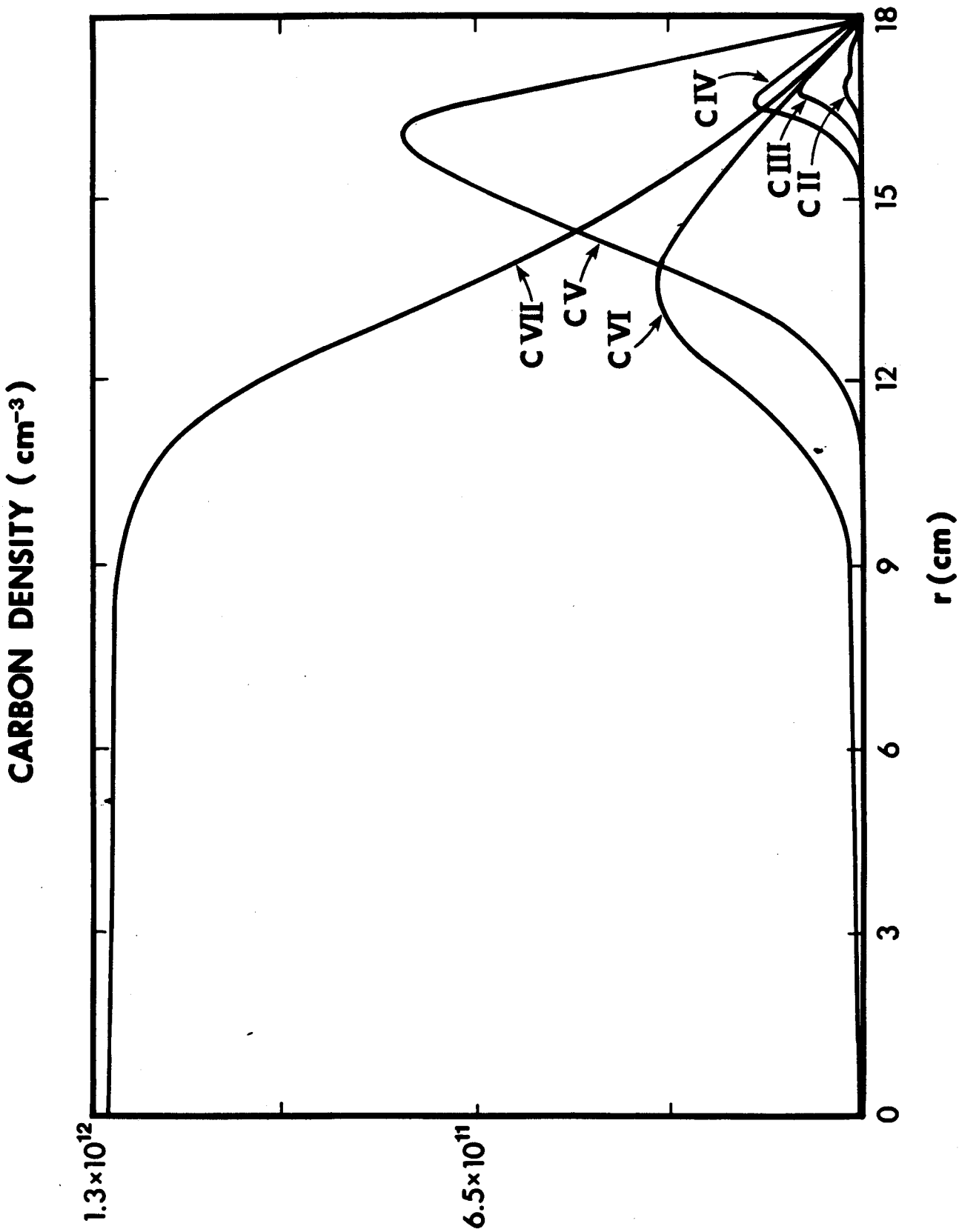
CARBON DENSITY (cm⁻³)
1.3×10¹²
6.5×10¹¹
0
3
6
9
12
15
18
r (cm)
C VII
C V
C VI
C IV
C III
C II

FIGURE 7

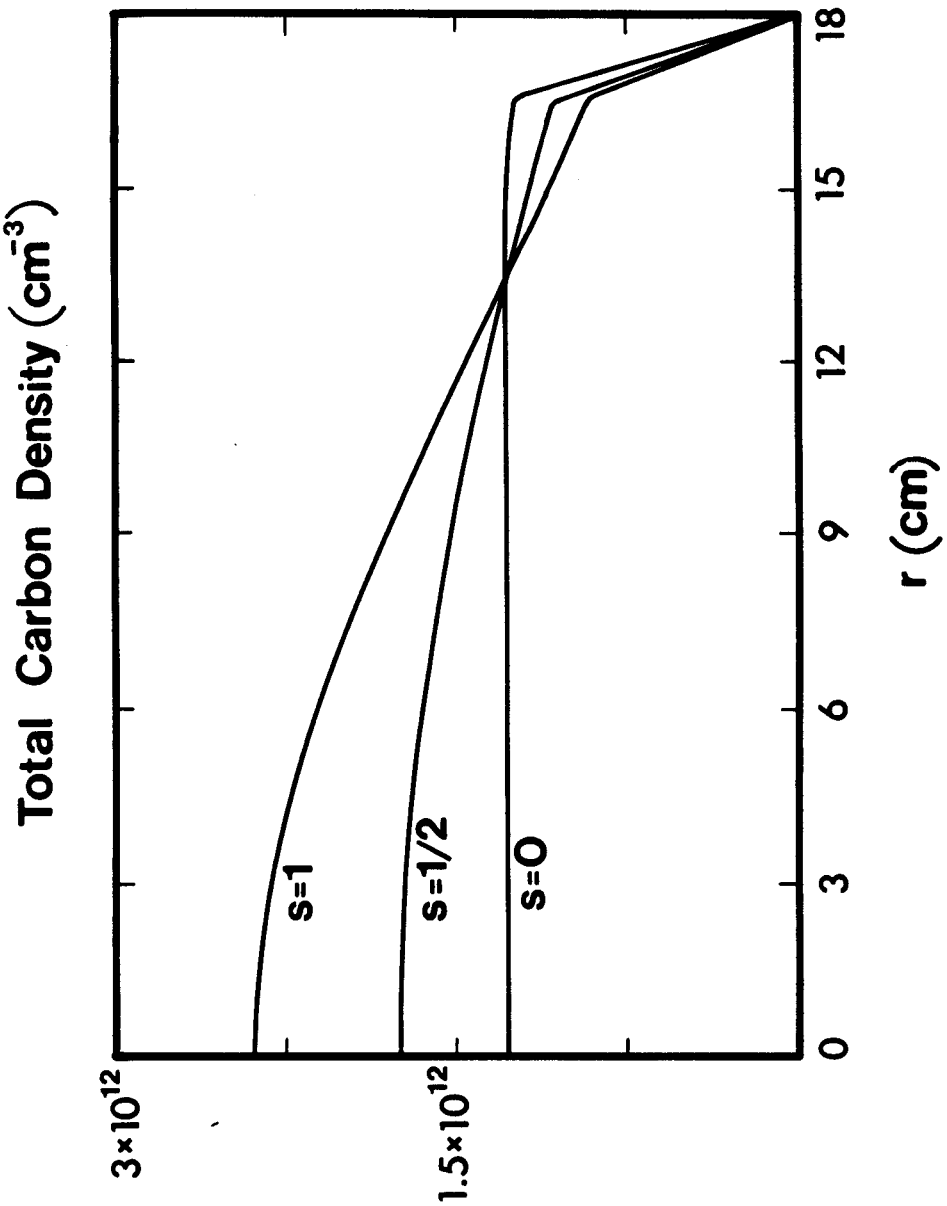
Total Carbon Density (cm^{-3})
3×10^{12}
1.5×10^{12}
0
3
6
9
12
15
18
r (cm)
s=1
s=1/2
s=0

FIGURE 8

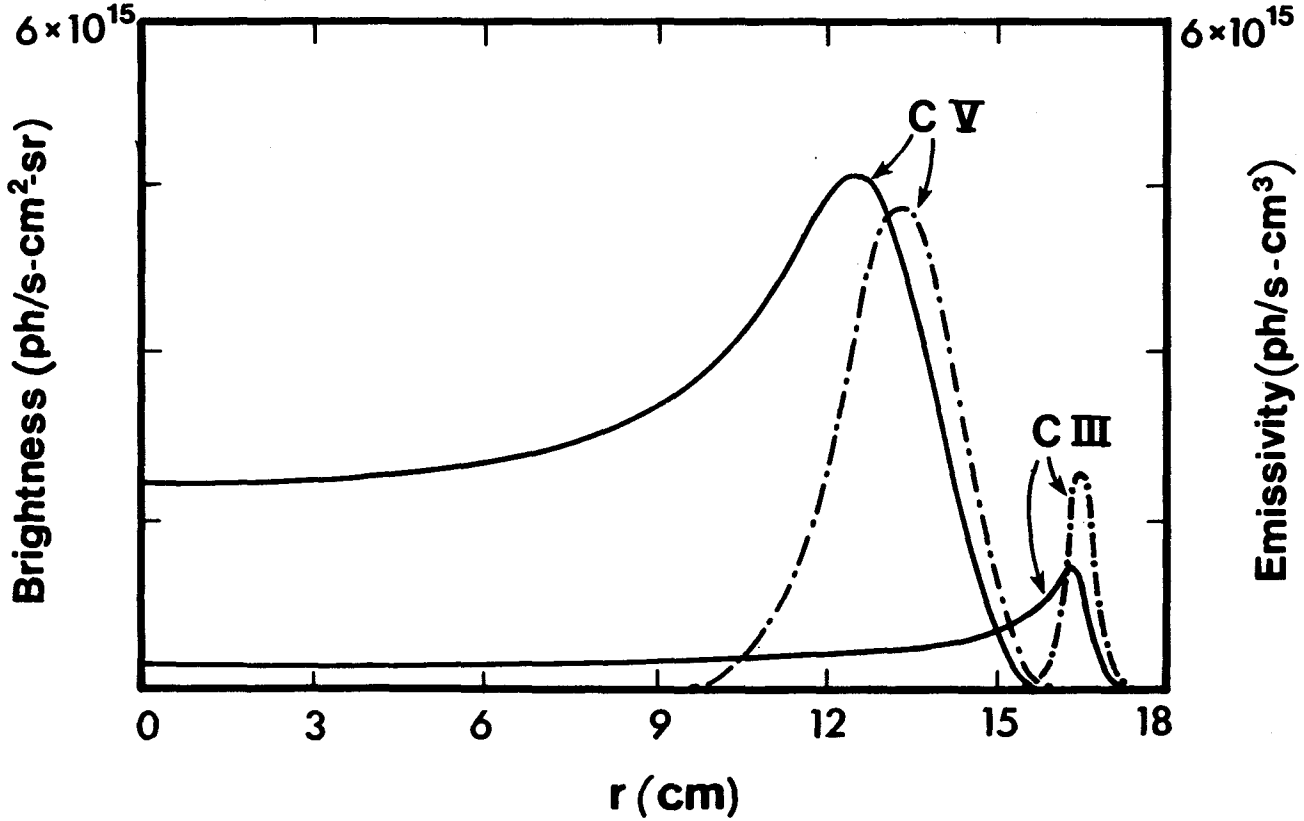
6×10^15
6×10^15
C V
C III
Brightness (ph/s-cm^2-sr)
Emissivity(ph/s-cm^3)
0
3
6
9
12
15
18
r (cm)

FIGURE 6

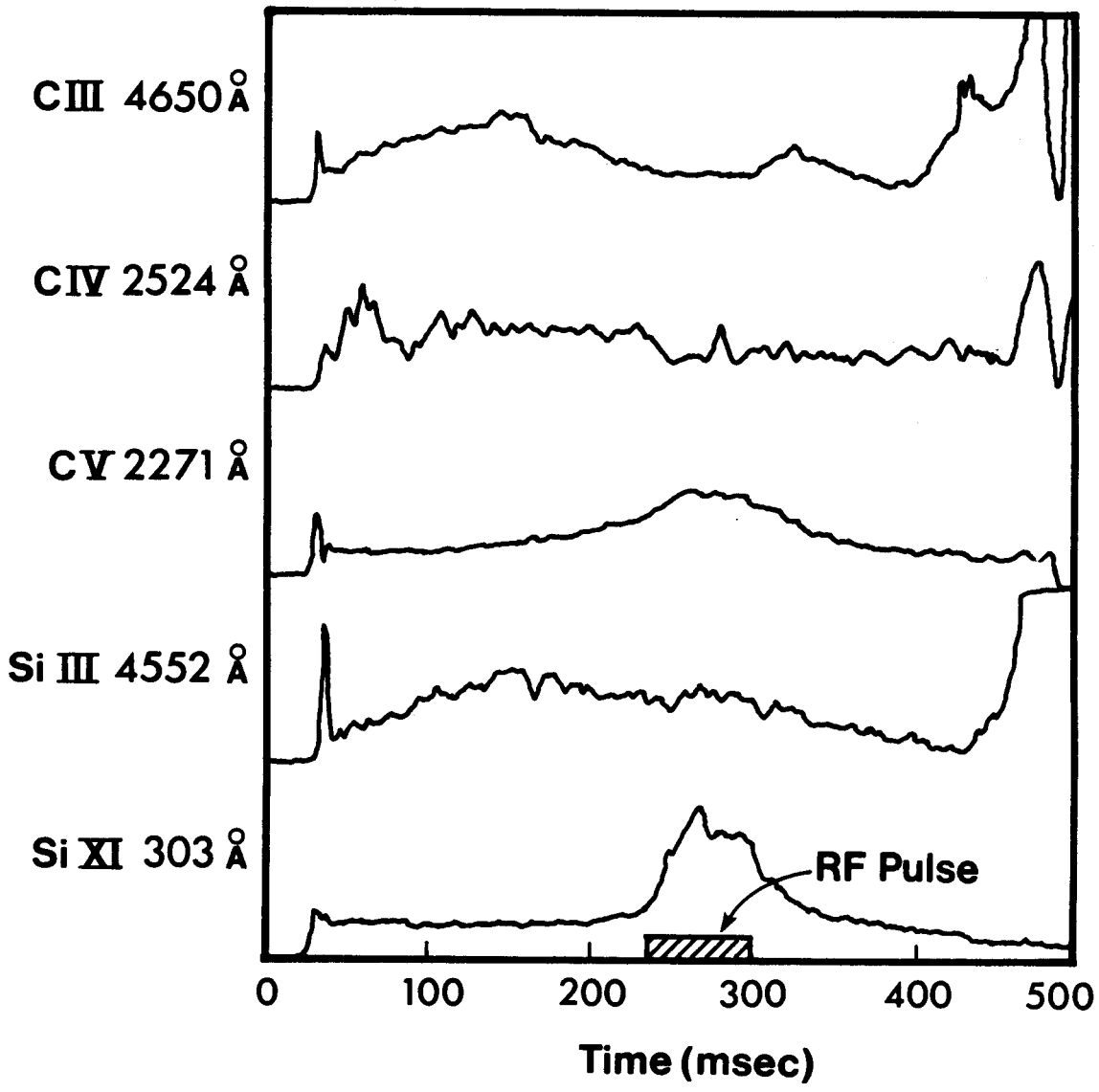
C III 4650 Å
C IV 2524 Å
C V 2271 Å
Si III 4552 Å
Si XI 303 Å
RF Pulse
0
100
200
300
400
500
Time (msec)

FIGURE 10

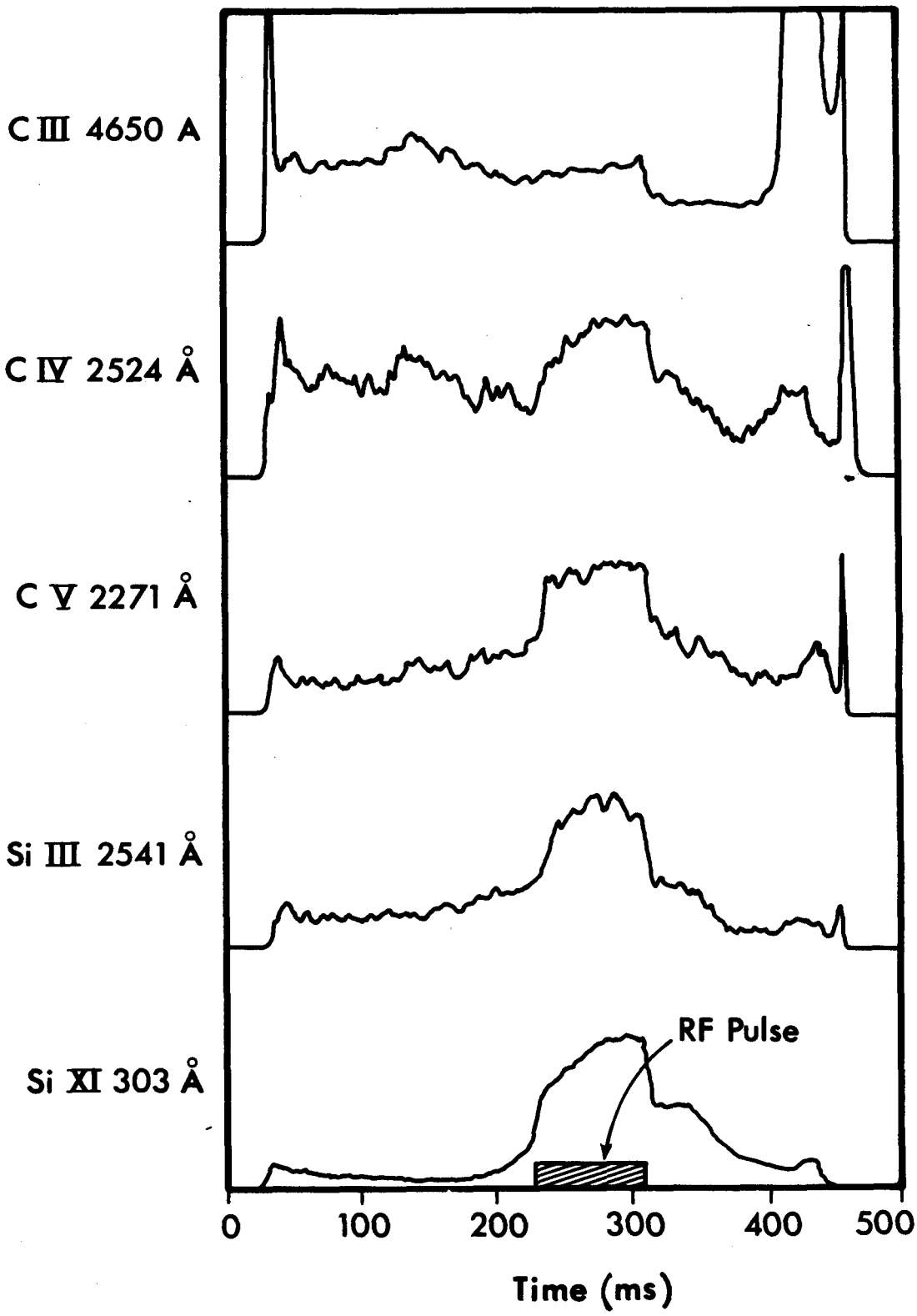
C III 4650 A
C IV 2524 Å
C V 2271 Å
Si III 2541 Å
Si XI 303 Å
RF Pulse
0
100
200
300
400
500
Time (ms)

FIGURE 11